Charge-density-wave phase transition in the quasi-one-dimensional conductor Nb_3Te_4

Tomoyuki Sekine, Yoshinari Kiuchi,* and Etsuyuki Matsuura
Institute of Physics, University of Tsukuba, Sakura-mura, Ibaraki 305, Japan

Kunimitsu Uchinokura
Department of Applied Physics, The University of Tokyo, Hongo, Bunkyo-ku, Tokyo 113, Japan

Ryozo Yoshizaki
Institute of Applied Physics, University of Tsukuba, Sakura-mura, Ibaraki 305, Japan
(Received 12 February 1987)

The phase transition of the quasi-one-dimensional conductor Nb_3Te_4 has been studied by electrical resistivity, magnetic susceptibility, and x-ray diffraction measurements. Two anomalies were observed at about 110 and 40 K in both the resistivity and the magnetic susceptibility data. Hysteresis was found at about 110 K, indicating that this phase transition is of first-order type. The x-ray study demonstrated clearly that the 110-K phase transition is accompanied by the appearance of superlattice reflections which are characterized by commensurate wave vectors $\mathbf{q}=\pm(\frac{1}{3}\mathbf{a}^*+\frac{1}{3}\mathbf{b}^*)+\frac{3}{7}\mathbf{c}^*$. This phase transition is due to charge-density-wave (CDW) formation. A possible crystal structure of the commensurate CDW state was discussed in terms of Landau theory; it has a $\sqrt{3}|\mathbf{a}|\times\sqrt{3}|\mathbf{a}|\times 7|\mathbf{c}|$ superlattice structure with C_3^1 ($P3$) symmetry. This structure with a $\sqrt{3}|\mathbf{a}|\times\sqrt{3}|\mathbf{a}|$ basal-plane unit cell minimizes the interchain interaction energy between the CDW's on the individual zigzag Nb chains.

I. INTRODUCTION

Quasi-one-dimensional conductors are intrinsically unstable against a $2\mathbf{k}_F$ lattice modulation, where $\mathbf{k}_F$ is the Fermi wave vector. Many of them undergo a structural phase transition, i.e., a Peierls transition, and a charge-density wave (CDW) is formed together with the lattice distortion. Below the transition temperature T_c a gap opens at the Fermi surface and then, in principle, the materials become semiconductors or insulators.

Recently considerable interest has been paid to Nb_3Te_4 together with the isostructural compounds Nb_3S_4 and Nb_3Se_4 because of their quasi-one-dimensional properties and the occurrence of superconductivity.[1,2] Nb_3Te_4 has a hexagonal structure and belongs to the space group C_{6h}^2 ($P6_3/m$) at room temperature.[3] As shown in Fig. 1, in a hexagonal unit cell there are three zigzag Nb chains running along the crystallographic c axis and there are eight Te atoms among the Nb chains. The distance between the Nb atoms along the zigzag chain is 2.973 Å which is comparable with the interatomic spacing of 2.86 Å in the pure Nb metal. The Nb chains are separated from one another by the Te atoms. And the interchain Nb distance of 3.854 Å is considerably larger. The charges, therefore, are carried along these zigzag Nb chains and these facts provide this crystal with its quasi-one-dimensional character.

Oshiyama[4] calculated the energy-band structures of the isostructural crystals Nb_3S_4, Nb_3Se_4, and Nb_3Te_4 using the self-consistent numerical-basis-set linear-combination-of-atomic-orbitals (LCAO) method. His calculation revealed that each of these crystals has three warped or undulating planar Fermi surfaces because of the existence of three zigzag Nb chains in a unit cell. It also showed that the widths of their conduction bands are in the range from 1.5 to 2.5 eV for the chain direction, while they are of the order of 0.1 eV for the direction perpendicular to the chain. The ratio of the conduction-band width along the chain direction to that along the perpendicular direction is about 19 for Nb_3Te_4, which is the largest among the three isostructural compounds. The effective-mass ratio of $m_\perp/m_\parallel$ was estimated to be 23 from the critical-magnetic-field ratio in the superconducting state,[2] where $m_\perp$ and $m_\parallel$ are the effective masses of the carriers perpendicular and parallel to the c axis, respectively. This is comparable to the value of the bandwidth ratio.[4] These facts suggest that these compounds have an anisotropy in the electrical conductivity, i.e., that they are quasi-one-dimensional conductors. However the warping or the undulation of

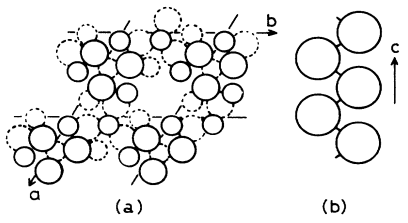

FIG. 1. Crystal structure of Nb_3Te_4. (a) View down the c (z) axis. Nb atoms are denoted by large circles and Te atoms by small circles. Atoms on the plane with $z=|\mathbf{c}|/4$ and $z=3|\mathbf{c}|/4$ are drawn by solid lines and dashed lines, respectively. (b) Zigzag Nb chains along the c axis (from Ref. 4).

their planar Fermi surfaces reflects the importance of the interchain interaction in these compounds.

Ishihara *et al.*[2,5] observed two anomalies at about 80 and 20 K in the electrical resistivity of Nb_3Te_4. Moreover the corresponding anomalies appear also in the thermoelectric power.[5] They pointed out that these anomalies of the resistivity may be due to CDW formation. Suzuki *et al.*[6] observed a superlattice structure which is characterized by commensurate wave vectors $\mathbf{q}=\frac{2}{3}\mathbf{a}^*\pm\frac{3}{7}\mathbf{c}^*$, in their notation, where $\mathbf{a}^*$ ($\mathbf{b}^*$) and $\mathbf{c}^*$ are the reciprocal vectors of the primitive unit-cell vectors $\mathbf{a}$ ($\mathbf{b}$) and $\mathbf{c}$ of the normal phase, respectively, at about 30 K by electron diffraction measurements.

In the present paper we investigate the phase transitions of Nb_3Te_4 by electrical resistivity, magnetic susceptibility, and x-ray diffraction measurements. We shall show clearly that the formation of the superlattice structure induces the high-temperature anomaly observed in the electrical resistivity. Hysteresis is observed around 110 K in both the electrical resistivity and the integrated intensity of the superlattice reflection at the point $(\frac{2}{3},-\frac{1}{3},\frac{3}{7})$ in reciprocal space. Moreover we shall discuss the phase transition at about 110 K in terms of Landau theory and also in terms of an interchain interaction between CDW's running on the individual Nb chains. A part of this study has briefly been reported previously.[7]

II. EXPERIMENTS

Nb_3Te_4 crystals were synthesized by the iodine-vapor transport method in sealed quartz tubes whose centers were kept at 1000 °C in a two-zone furnace with a temperature gradient of 3 °C/cm.[2] A powder of Nb and Te in stoichiometric proportion was located at the centers of the quartz tubes. The crystals obtained were needlelike with a maximum size of about 2 cm in length and 0.2×0.2 mm^2 in cross section. In order to study the correlation between the anomaly observed in the electrical resistivity and the formation of the superlattice structure, we measured the electrical resistivity and x-ray diffraction on the same sample.

The dc electrical resistivity was measured along the chain direction (the c axis) using the four-probe technique. Thin gold wires were attached to the sample with silver paste.

The static magnetic susceptibility was measured at 30 kG by a superconducting quantum-interference device (SQUID) susceptometer (S.H.E. Corporation model VTS-50). The crystallographic axes of the samples were not arrayed in the same directions because the crystals were very small. The typical amount of the samples used in the magnetic susceptibility measurements was about 30 mg.

The x-ray measurement was carried out using a four-circle goniometer (Huber Ltd. Eulerian Cradle 512). The Mo $K\alpha$ radiation was provided by a rotating-anode x-ray generator (JEOL Ltd. JRX-12HC) with the input power of 46 kV, 140 mA. A pure Ge solid-state detector (SSD, Aptec Engineering Ltd. PS-25) was used together with a multichannel analyzer. The whole system was controlled by a computer. In the x-ray measurement the samples were cooled down to about 10 K by a continuous-He-gas-flow cryostat (Oxford Instrument Ltd.).

III. EXPERIMENTAL RESULTS

The electrical resistivity along the c axis as a function of temperature is shown in Fig. 2. As the temperature is lowered from room temperature, the resistivity decreases monotonically, which demonstrates the metallic nature of the material. At about 110 K the resistivity begins to increase and then has a peak at about 90 K. Moreover another anomaly is observed at about 40 K. The characteristics of this temperature-dependent resistivity are almost the same as those reported by Ishihara *et al.*[2,5] But the residual resistivity ratio (4.2) of our sample is larger than that (about 3) of Ishihara *et al.* Our data reveal clearly the existence of a hysteresis near 100 K. At low temperatures the resistivity shows metallic behavior again, and we confirmed that a sudden decrease of the resistivity appeared below 2.8 K because of the existence of the superconducting transition.[1,2]

Figure 3 shows the magnetic susceptibility of Nb_3Te_4 during the heating run. Paramagnetism increases gradually with decreasing temperature down to 105 K. The magnetic susceptibility has anomalies around 105 and 45 K. At low temperatures we can see a Curie contribution due to paramagnetic impurities.

By x-ray diffraction, we observed commensurate superlattice reflections around the reciprocal point (0,0,0) at 32.5 K. These superlattice reflections are due to the condensation of the lattice modulations with the following wave vectors:

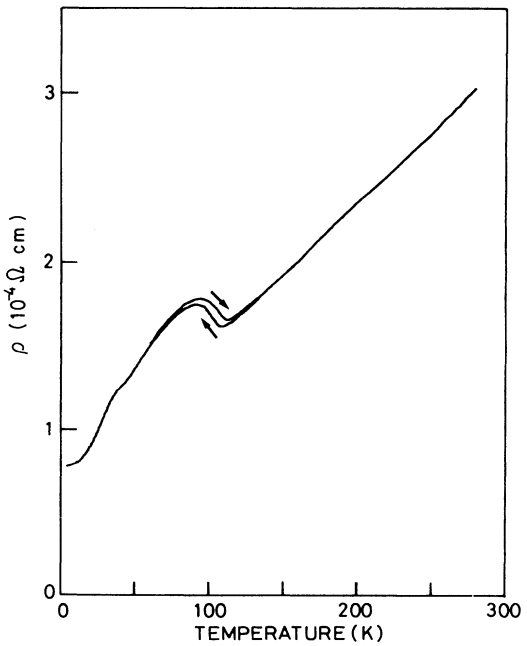

FIG. 2. Temperature dependence of the electrical resistivity of Nb_3Te_4 in the same sample as used in the x-ray diffraction measurement.

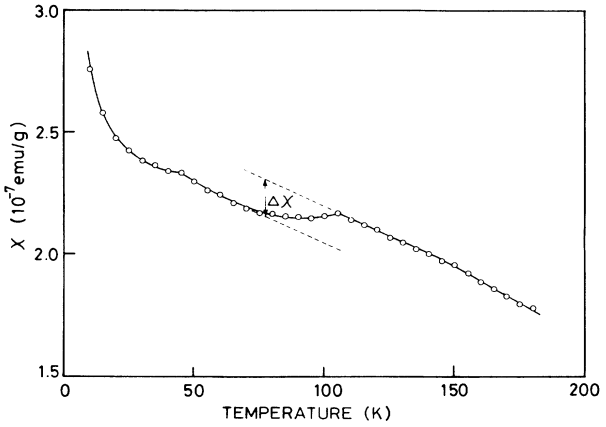

FIG. 3. Temperature dependence of the magnetic susceptibility of Nb_3Te_4 in the heating run.

$$
\begin{aligned}
&\mathbf{q}_1=\tfrac{1}{3}\mathbf{a}^*+\tfrac{1}{3}\mathbf{b}^*+\tfrac{3}{7}\mathbf{c}^*,\quad \mathbf{q}_1^*=-\mathbf{q}_1\ ,\\
&\mathbf{q}_2=-\tfrac{1}{3}\mathbf{a}^*+\tfrac{2}{3}\mathbf{b}^*+\tfrac{3}{7}\mathbf{c}^*,\quad \mathbf{q}_2^*=-\mathbf{q}_2\ ,\\
&\mathbf{q}_3=-\tfrac{2}{3}\mathbf{a}^*+\tfrac{1}{3}\mathbf{b}^*+\tfrac{3}{7}\mathbf{c}^*,\quad \mathbf{q}_3^*=-\mathbf{q}_3\ ,\\
&\mathbf{q}_4=-\tfrac{1}{3}\mathbf{a}^*-\tfrac{1}{3}\mathbf{b}^*+\tfrac{3}{7}\mathbf{c}^*,\quad \mathbf{q}_4^*=-\mathbf{q}_4\ ,\\
&\mathbf{q}_5=\tfrac{1}{3}\mathbf{a}^*-\tfrac{2}{3}\mathbf{b}^*+\tfrac{3}{7}\mathbf{c}^*,\quad \mathbf{q}_5^*=-\mathbf{q}_5\ ,\\
&\mathbf{q}_6=\tfrac{2}{3}\mathbf{a}^*-\tfrac{1}{3}\mathbf{b}^*+\tfrac{3}{7}\mathbf{c}^*,\quad \mathbf{q}_6^*=-\mathbf{q}_6\ .
\end{aligned}
\tag{1}
$$

Here $\mathbf{q}_i^*$ $(=-\mathbf{q}_i)$ is the wave vector obtained from $\mathbf{q}_i$ using the time-reversal operation. These wave vectors are shown in Fig. 4. They are not independent of one another. $\mathbf{q}_i$ $(\mathbf{q}_i^*)$, $\mathbf{q}_{i+2}$ $(\mathbf{q}_{i+2}^*)$ and $\mathbf{q}_{i+4}$ $(\mathbf{q}_{i+4}^*)$ are equivalent, where $i=1$ and 2. Although the wave vectors reported by Suzuki *et al.*[6] have different notation, their superlattice reflections would have the same $\mathbf{q}$ values as ours if they had used the correct reciprocal unit-cell vectors of the hexagonal lattice. Figure 5 shows the temperature dependence of the integrated intensity of the $(\frac{2}{3},-\frac{1}{3},\frac{3}{7})$ superlattice reflection in the same sample as used in the electrical resistivity measurement. At first, the sample was cooled down to about 10 K from room temperature at a cooling rate of about 7.3 K/min. Then we measured the integrated intensity of the superlattice reflection up to 150 K during the heating run (the rate was about 0.3 K/min during heating and the temperature was set constant for 15 min during the measurement). In Fig. 5 the closed squares denote the integrated intensity during the first heating run. The measurement was performed again during the second cooling (open circles) and heating (solid circles) runs, with the cooling and heating rates of about 0.4 K/min. The integrated intensities in the second cooling and heating runs show the existence of the hysteresis. The transition temperatures in the cooling and heating runs were determined to be 108 and 111 K, respectively, by extrapolating the data toward the background. They correspond to the temperatures at the point of increase of the electrical resistivity. A clear difference between the integrated intensities of the superlattice reflection in the first heating run and those in the second heating run was found below 80 K. Moreover we found that the transition temperature of the high-temperature phase transition depends on individual samples.

We were able to observe no essential change in the integrated intensity of the superlattice reflection at the reciprocal point $(\frac{2}{3},-\frac{1}{3},\frac{3}{7})$ around 40 K. And we did not observe new superlattice reflection below 40 K. This fact cannot completely deny the existence of another phase

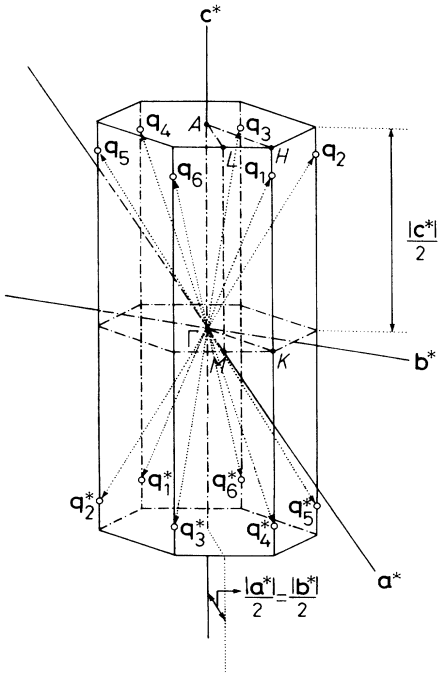

FIG. 4. The wave vectors of the superlattice reflections in the Brillouin zone.

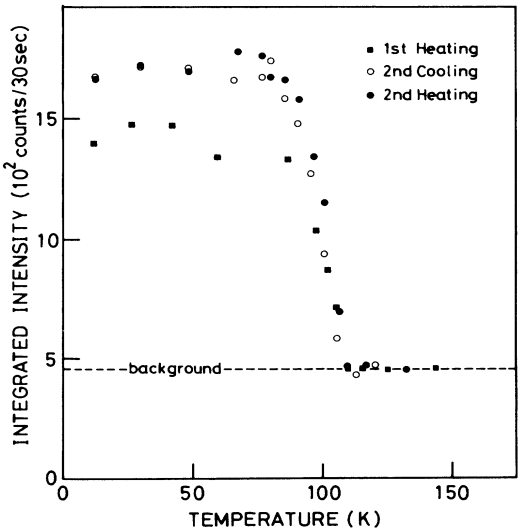

FIG. 5. Temperature dependence of the integrated intensity of the superlattice reflection at the reciprocal point $(\frac{2}{3},-\frac{1}{3},\frac{3}{7})$. It was measured using a $2\theta-\omega$ scan method.

transition around 40 K, because it is impossible to examine the whole reciprocal space in detail.

IV. DISCUSSION

The temperature of the point of increase of the electrical resistivity coincides exactly with that of the appearance of the superlattice reflection at the point $(\frac{2}{3}, -\frac{1}{3}, \frac{3}{7})$ in reciprocal space. This result demonstrates clearly that the anomaly at about 110 K in the electrical resistivity is due to the formation of the superlattice structure. The existence of the hysteresis at about 110 K in the electrical resistivity and in the integrated intensity of the superlattice reflection indicates that the phase transition is first order. The integrated intensity of the superlattice reflection depends strongly on the cooling rate, which indicates that the domains are formed in the low-temperature phase below about 110 K. This fact is consistent with the results of the electron diffraction measurement.[6]

A calculation of the energy-band structure of Nb_3Te_4 has been performed by Oshiyama.[4] It shows that there exist three Fermi surfaces which consist of slightly warped planelike sheets perpendicular to the c axis. This is due to the existence of three zigzag Nb chains interacting with one another in each unit cell. The wave vectors of the two outer Fermi surfaces along the c direction are in the Brillouin zone in the range from about $0.25\mathbf{c}^*$ to $0.17\mathbf{c}^*$. The component $3\mathbf{c}^*/7$ of the superlattice reflection is nearly equal to twice the Fermi wave vectors of the two outer Fermi surfaces. This fact indicates that the formation of the superlattice structure at about 110 K is due to CDW formation. The interchain interaction introduces the warping of the Fermi surfaces,[4] so that the wave vector of the CDW may have the component $\frac{1}{3}\mathbf{a}^* + \frac{1}{3}\mathbf{b}^*$ in the hexagonal a^*-b^* plane. This will be discussed later in detail.

We tried to detect the nonlinearity of the dc conductivity in the electric field from 0.1 mV/cm to 40 V/cm by continuous and pulse methods and also measured the ac conductivity in the frequency range from 10 Hz to 13 MHz. But no effect due to the motion of the CDW was observed. This is consistent with the fact that the CDW of Nb_3Te_4 is commensurate.

As shown in Fig. 3, in the magnetic susceptibility of Nb_3Te_4 we observed two anomalies around 105 and 45 K, where the paramagnetism decreased. The CDW formation breaks a part of the Fermi surfaces where the nesting condition is satisfied. The decrease of the paramagnetism at about 105 K can be understood in terms of the decrease of the area of the Fermi surfaces due to CDW formation. The Pauli paramagnetism is proportional to the density of states at the Fermi surfaces:[8]

$$\chi_{\text{Pauli}} = \mu_B^2 D(E_F) N_a / M \text{ emu/g} , \tag{2}$$

where μ_B is the Bohr magneton (erg/G), $D(E_F)$ is the density of states (states/erg molecule) at the Fermi surfaces, N_a is the Avogadro's number (mol^{-1}), and M is the weight per mol (g/mol). From Fig. 3 we estimate the decrease of the paramagnetism as $\Delta\chi = 0.15 \times 10^{-7}$ emu/g. Using this value and Eq. (2), we obtain the decrease of the density of states at the Fermi surfaces as $D(E_F) = 0.23 \times 10^{12}$ states/(erg molecule). Oshiyama[4] calculated $D(E_F) = 1.42 \times 10^{12}$ states/(erg molecule). About 16% of the density of states at the Fermi surfaces disappeared owing to CDW formation at about 110 K. Under the assumption that CDW formation at about 110 K occurs only in one sheet out of the three sheets and that each sheet has almost the same density of states, the sheet concerned loses about 50% of the density of states.

Let us consider the crystal structure in the commensurate CDW state below about 110 K in terms of phenomenological Landau theory. It may be allowable for us to consider that the crystal is transformed directly from the normal phase to the commensurate one around 110 K and the phase transition is of weakly first-order type. Consequently the Landau theory of the second-order phase transition may be applied to the present case.

We take into consideration four inequivalent wave vectors, $\mathbf{q}_1$, $\mathbf{q}_1^*$, $\mathbf{q}_4$, and $\mathbf{q}_4^*$, which constitute the star of $\mathbf{q}_1$. The small group at the K-H line is C_3. The lattice distortions relative to the high-temperature phase are given by the vector[9]

$$\mathbf{u} = \text{Re}(\Psi_1 \mathbf{e}_1 + \Psi_2 \mathbf{e}_2) . \tag{3}$$

Here $\mathbf{e}_1$ and $\mathbf{e}_2$ $(= C_{2z}\mathbf{e}_1)$ are the basis vectors of the group of the wave vectors $\mathbf{q}_1$ and $\mathbf{q}_4$, respectively. The transformation properties of the components Ψ_i of the complex order parameters with respect to the elements of the space group C_{6h}^2 are given in the Appendix. We assume that the phonon mode responsible for the high-temperature CDW phase transition is a mode with A representation, which is a one-dimensional representation of the small group C_3. The basis vectors $\mathbf{e}_i$, therefore, belong to the A representation. This assumption will be discussed later. The free energy is invariant with respect to the symmetry transformation of the normal phase and can be described as follows:

$$F = a_0(|\Psi_1|^2 + |\Psi_2|^2) + a_1(|\Psi_1|^4 + |\Psi_2|^4) + a_2|\Psi_1|^2|\Psi_2|^2 + a_3(|\Psi_1|^6 + |\Psi_2|^6)$$
$$+ a_4(|\Psi_1|^2|\Psi_2|^4 + |\Psi_1|^4|\Psi_2|^2) + a_5(\Psi_1^3\Psi_2^{*3} + \Psi_1^{*3}\Psi_2^3) . \tag{4}$$

We assume as is general practice that only a_0 is temperature dependent as follows:

$$a_0 = a'(T - T_0) , \tag{5}$$

where $a' > 0$ and all other coefficients are temperature independent. By substituting

$$\Psi_1 = \Phi_1 \exp(i\varphi_1) , \tag{6a}$$

and

$$\Psi_2=\Phi_2\exp(i\varphi_2)\ , \tag{6b}$$

where $\Phi_1\geqq 0$ and $\Phi_2\geqq 0$, into Eq. (4), the free energy F becomes

$$F=a(\Phi_1^2+\Phi_2^2)-b(\Phi_1^2+\Phi_2^2)^2+c\Phi_1^2\Phi_2^2+d(\Phi_1^2+\Phi_2^2)^3 +e(\Phi_1^2\Phi_2^4+\Phi_1^4\Phi_2^2)+f\Phi_1^3\Phi_2^3\cos[3(\varphi_1-\varphi_2)]\ , \tag{7}$$

where $a=a_0$, $b=-a_1$, $c=-2a_1+a_2$, $d=a_3$, $e=-3a_3+a_4$, and $f=2a_5$. Moreover using the following notations:

$$|\Psi_1|=\Phi_1=\phi\cos\theta \quad\text{and}\quad |\Psi_2|=\Phi_2=\phi\sin\theta\ , \tag{8}$$

where $\phi\geqq 0$ and $0\leqq\theta\leqq\pi/2$, Eq. (7) is rewritten as

$$F=a\phi^2-\left[b-\frac{c}{4}\sin^2(2\theta)\right]\phi^4 +\left[d+\frac{e}{4}\sin^2(2\theta)+\frac{f}{8}\cos[3(\varphi_1-\varphi_2)]\sin^3(2\theta)\right]\phi^6\ . \tag{9}$$

Minimizing F with respect to θ gives

$$\phi^4\{c+\phi^2[e+\tfrac{3}{4}f\cos[3(\varphi_1-\varphi_2)]\sin(2\theta)]\}\times\sin(4\theta)=0\ . \tag{10}$$

We obtain four solutions. (1) $\phi=0$. This can be stated as

$$\Phi_1=\Phi_2=0\ . \tag{11}$$

(2) $\theta=0$. This can be stated as

$$\Phi_1=\phi \quad\text{and}\quad \Phi_2=0\ . \tag{12}$$

The free energy F becomes

$$F=a\phi^2-b\phi^4+d\phi^6\ . \tag{13}$$

Since experimentally the transition is first order, we assume $b>0$ and $d>0$. Then ϕ and the transition temperature T_c are given by

$$\phi=\left[\frac{b+(b^2-3ad)^{1/2}}{3d}\right]^{1/2} \tag{14}$$

and

$$T_c=T_0+\frac{b^2}{4a'd}\ . \tag{15}$$

(3) $\theta=\pi/2$. This is equal to

$$\Phi_1=0 \quad\text{and}\quad \Phi_2=\phi\ . \tag{16}$$

Here ϕ and the transition temperature T_c are given by Eqs. (14) and (15), respectively. (4) $\theta=\pi/4$. This is equal to

$$\Phi_1=\Phi_2=\phi/\sqrt{2}\ . \tag{17}$$

Equation (9) is rewritten as

$$F=a\phi^2-\left[b-\frac{c}{4}\right]\phi^4+\left[d+\frac{e}{4}+\frac{f}{8}\cos[3(\varphi_1-\varphi_2)]\right]\phi^6\ . \tag{18}$$

By minimizing F with respect to $(\varphi_1-\varphi_2)$, we obtain

$$\varphi_1-\varphi_2=0,\pm 2\pi/3 \quad\text{if } f<0\ , \tag{19a}$$

or

$$\varphi_1-\varphi_2=\pi,\pm\pi/3 \quad\text{if } f>0\ . \tag{19b}$$

Then ϕ and T_c are given as

$$\phi=\left[\frac{(b-c/4)+[(b-c/4)^2-3a(d+e/4-|f|/8)]^{1/2}}{3(d+e/4-|f|/8)}\right]^{1/2} \tag{20}$$

and

$$T_c=T_0+\frac{(b-e/4)^2}{4a'(d+e/4-|f|/8)}\ . \tag{21}$$

Here we assume $(b-c/4)>0$ and $(d+e/4-|f|/8)>0$, because experimentally the phase transition is first order.

Apparently solution (1) corresponds to the normal phase of Nb_3Te_4 above about 110 K. Solutions (2) and (3) are degenerate and therefore they form domains. In the solutions (2)–(4) the primitive unit-cell vectors of the commensurate phase are given as

$$\mathbf{a}'=\mathbf{a}+2\mathbf{b},\quad \mathbf{b}'=-2\mathbf{a}-\mathbf{b},\quad \mathbf{c}'=7\mathbf{c}\ . \tag{22}$$

Suzuki *et al.*[6] have observed distinct striped domains using the dark-field images of electron microscopy, which were obtained using the superlattice diffraction beam. In our x-ray diffraction experiment the observed dependence of the integrated intensity of the superlattice reflection on the cooling rate of the sample also suggests the existence of the domains below about 110 K. The bright domain can be assigned to solution (2) and the dark domain to solution (3), or vice versa.

The electron microscopy of Suzuki *et al.*[6] showed that in this domain structure the distinctly bright domains and dark ones alternately repeat themselves side by side with two orientations in crystallographically equivalent directions. Their boundaries are sharp and straight lines. They face each other with an angle of about 77° on the $(1\bar{1}.0)$ plane. We must note that this angle agrees with that between the vectors $\mathbf{Q}_1$ and $\mathbf{Q}_2$, where $\mathbf{Q}_1=3\mathbf{a}+3\mathbf{b}+7\mathbf{c}$ and $\mathbf{Q}_2=3\mathbf{a}+3\mathbf{b}-7\mathbf{c}$. Here we used $|\mathbf{a}|=|\mathbf{b}|=10.671$ Å and $|\mathbf{c}|=3.6468$ Å.[3] This fact indicates that the commensurate superlattice structure has $3|\mathbf{a}|\times 7|\mathbf{c}|$ on the $(1\bar{1}.0)$ plane. As will be point-

ed out later, the domains with the order parameters Ψ_1 and Ψ_2 correspond to the states having different phases, $-2\pi/3$ and $+2\pi/3$, respectively, between the three zigzag Nb chains in the a-b plane. Because of the large difference of the phases between these domains, a large strain is expected to accumulate in the domain walls. We can easily imagine a strong repulsive interaction between the adjacent domain walls. The strong repulsive interaction would tend to keep the domain walls parallel to each other.[10] The domain walls usually should be parallel to high symmetry planes. In this case they are parallel to the $(11.\bar{1})$ and (11.1) planes of the commensurate structure. We, therefore, think that the results of the electron diffraction are consistent with our proposed theory.

In the solution (4) the states with the phases $\varphi_1-\varphi_2=0$, $+2\pi/3$, and $-2\pi/3$ become degenerate when $f<0$ or the states with $\varphi_1-\varphi_2=\pi$, $+\pi/3$, and $-\pi/3$ become degenerate when $f>0$, but these domains have the same diffraction pattern. Consequently in this case we should not observe the striped domains by dark-field electron microscopy and the dependence of the integrated intensity of the superlattice reflection on the cooling rate by x-ray diffraction. We, therefore, conclude that the commensurate CDW state of Nb_3Te_4 corresponds to solutions (2) and (3) in the temperature region between about 40 and 110 K.

In solutions (2) and (3) the sixth term locking the phase φ_1 or φ_2 of the order parameter in Eq. (4) is zero. We did not take into account the lock-in terms which lock commensurately the wave vector along the c^* axis and can be described in the form

$$g_1 \operatorname{Re}[(\Psi_1\Psi_2)^7]+g_2 \operatorname{Re}(\Psi_1^{21}+\Psi_2^{21}) . \tag{23}$$

In solutions (2) and (3) only the second term is effective and therefore we obtain 21 solutions for the phase φ_1 or φ_2,

$$\varphi_1 \text{ or } \varphi_2=2n\pi/21 \quad \text{if } g_2<0 , \tag{24a}$$

or

$$\varphi_1 \text{ or } \varphi_2=2(n+1)\pi/21 \quad \text{if } g_2>0 , \tag{24b}$$

where $n=0,1,\ldots,20$. They all are degenerate and differ from one another only in the location of the origin of the commensurate phase. In fact in addition to this lock-in term, many impurities in the crystal pin the phase. The states with different phases form domains whose boundaries have phase slips. These domains have the same diffraction pattern, but the phase-slip walls may have weak strain because the phase slip easily occurs with a small phase change. Recently Suzuki *et al.*[11] observed that a number of tiny, irregularly formed and slightly dark regions emerged in the bright domains of the distinct striped-domain structure. We identified the tiny regions as the phase-slip walls between the different phases φ_1 or φ_2 of the order parameter Ψ_1 or Ψ_2. Since the weak strain may accumulate in the phase-slip walls, the repulsive interaction between the adjacent phase-slip walls may be weak. Many tiny and dark regions, therefore, can be observed irregularly and faintly in the bright domains of the distinct striped-domain structure.[10,11]

Let us discuss the structure of the commensurate CDW state from a different point of view. Figure 6(a) shows the structure of Nb_3Te_4 viewed along the c axis in the normal phase. There are three zigzag Nb chains in a unit cell and the Nb atoms form a triangle on the c plane. The conduction electrons of Nb_3Te_4 originate from the d electrons of the Nb atoms[4] and we can imagine that the quasi-one-dimensional conduction occurs along these chains. Peierls distortion, therefore, is induced along these chains. The energy-band calculation of Oshiyama on this crystal revealed warped or undulating planar Fermi surfaces, and the interaction between the chains has been suggested as its origin. We think that it causes the ordering of the phases of the CDW's on the individual chains, and that this leads to the appearance of the a^*-b^* component of the superlattice wave vector.

The main atomic displacements which are responsible for CDW phase transition around 110 K, therefore, are on the Nb atoms. It may be permissible to assume that the Te atoms do not move at this phase transition. The displacements of the Nb atoms in the jth ($j=1,2,3$) chain of the mth bundle of the three zigzag Nb chains, where the mth $[m=(m_1,m_2)]$ bundle constructs a unit cell at $\mathbf{r}=m_1\mathbf{a}+m_2\mathbf{b}$ on the a-b plane, are expressed as

$$\mathbf{u}_j^m(R(l))=\operatorname{Re}\{\zeta_j^m(R(l))\mathbf{e}_j^m \exp[iq_z R(l)]\} , \tag{25}$$

where $q_z=3\,|\,\mathbf{c}^*\,|\,/7$, $R(l)=l\,|\,\mathbf{c}\,|$, l is an integer, $\mathbf{e}_j^m$ is the basis vector of the jth chain of the mth bundle, and $\zeta_j^m(R(l))$ is the complex order parameter for the jth chain of the mth bundle of the three chains. We take $\zeta_j^m(z)$ to be independent of z and write

$$\zeta_j^m(z)=\alpha \exp[i\gamma_j+i(m_1q_x\,|\,\mathbf{a}\,|+m_2q_y\,|\,\mathbf{b}\,|)] . \tag{26}$$

Here $\alpha>0$. The three chains ($j=1,2,3$) are located at the corners of the triangle, as shown in Fig. 6(a). The nearest-neighbor interchain interaction energy is written as[12–14]

$$F_{\text{int}}=\eta\sum_{i,j}\sum_{m,n}\int dz \operatorname{Re}[\zeta_i^m(z)\zeta_j^{n*}(z)]$$

$$=NL\eta\alpha^2[\cos(\gamma_1-\gamma_2)+\cos(\gamma_2-\gamma_3)+\cos(\gamma_3-\gamma_1)$$

$$+\cos(\gamma_1-\gamma_2+2q\,|\,\mathbf{a}\,|)+\cos(\gamma_2-\gamma_3-q\,|\,\mathbf{a}\,|)+\cos(\gamma_3-\gamma_1-q\,|\,\mathbf{a}\,|)] . \tag{27}$$

Here N is the number of the bundles of chains in the crystal and L is the length of the crystal along the c direction. We assume $q_x = q_y = q$ and $\eta > 0$, because the interchain interaction originates mainly from a repulsive Coulomb interaction between adjacent CDW's. The interchain interaction energy F_{int} is minimized in the following four cases:

$$\text{(A)}\ q\,|\mathbf{a}| = 0\ , \qquad \gamma_1-\gamma_2=\gamma_2-\gamma_3=\gamma_3-\gamma_1=+2\pi/3\ . \tag{28}$$

$$\text{(B)}\ q\,|\mathbf{a}| = 0\ , \qquad \gamma_1-\gamma_2=\gamma_2-\gamma_3=\gamma_3-\gamma_1=-2\pi/3\ . \tag{29}$$

$$\text{(C)}\ q\,|\mathbf{a}| = +2\pi/3\ , \qquad \gamma_1-\gamma_2=\gamma_2-\gamma_3=\gamma_3-\gamma_1=-2\pi/3\ . \tag{30}$$

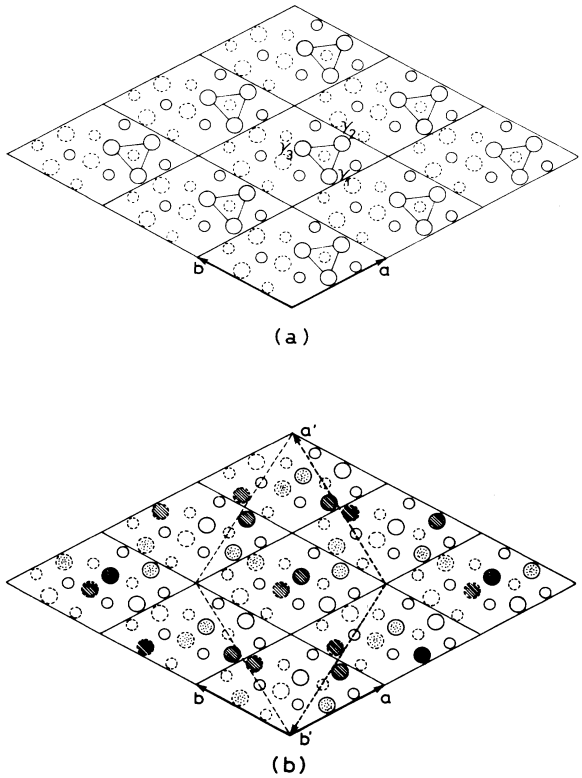

FIG. 6. Crystal structures of the normal phase (a) and the most possible commensurate CDW state (b) of Nb_3Te_4 viewed along the c axis. Nb atoms are denoted by large circles and Te atoms by small circles. Atoms on the plane with $z = |\mathbf{c}|/4$ and $z = 3|\mathbf{c}|/4$ are drawn by solid lines and dashed lines, respectively. In (a), γ_j $(j=1,2,3)$ denotes the phase of the jth zigzag Nb chain on the mth $[m=(m_1,m_2)]$ bundle of the three chains at $\mathbf{r}=m_1\mathbf{a}+m_2\mathbf{b}$. In the CDW states, the phase differences of the CDW's among ○, ◉, and ◎, at Nb positions on the $z = |\mathbf{c}|/4$ plane are $\mp 2\pi/3$. The symbols ◌, ◉, and ◎ indicate that the Nb atoms on the $z = 3|\mathbf{c}|/4$ plane belong to the same zigzag chains as ○, ◉, and ◎. The vectors $\mathbf{a}$ and $\mathbf{b}$ exhibit the unit cell on the a-b plane in the normal state, and $\mathbf{a}'$ and $\mathbf{b}'$ show the unit cell in the commensurate CDW state.

$$\text{(D)}\ q\,|\mathbf{a}| = -2\pi/3\ , \qquad \gamma_1-\gamma_2=\gamma_2-\gamma_3=\gamma_3-\gamma_1=+2\pi/3\ . \tag{31}$$

They each give the same F_{int} value. Cases (C) and (D) correspond, respectively, to solution (2) of the above-mentioned Landau theory, where the CDW with $\mathbf{q}_1$ is created, and solution (3), where the CDW with $\mathbf{q}_4$ is created. In the commensurate phase of Nb_3Te_4 cases (C) and (D) are realized. Cases (C) and (D) are displayed in Fig. 6(b).

In view of the electronic band structure, the interchain interaction causes the warping of the Fermi surfaces and the nesting vector has the component $\frac{1}{3}\mathbf{a}^*+\frac{1}{3}\mathbf{b}^*$ on the a^*-b^* plane. This may correspond to the warping of the Fermi surfaces obtained by Oshiyama's band calculation.[4]

In the present Landau theory solutions (2) and (3) come from the condensation of the A-mode lattice vibration (coupled with the CDW) at $\mathbf{q}_1$ and $\mathbf{q}_4$, respectively. These structures correspond to cases (C) and (D) where the interchain interaction energy between CDW's running on the individual chains is minimized. In other words, it is feasible that the phonon mode with A symmetry is responsible for the high-temperature CDW phase transition in Nb_3Te_4. The present model reveals clearly that the commensurate structure has a $\sqrt{3}|\mathbf{a}| \times \sqrt{3}|\mathbf{a}|$ basal-plane unit cell.

In solutions (2) and (3) the crystal has a three-fold rotation operator. We can determine that the space group of the commensurate CDW state is C_3^1 $(P3)$. The unit cell becomes $\sqrt{3}|\mathbf{a}| \times \sqrt{3}|\mathbf{a}| \times 7|\mathbf{c}|$. On the other hand, in solution (4) the crystal structure also has a space group of C_3^1 $(P3)$.

The low-temperature anomaly was observed at about 40 K by the electrical-resistivity measurement (Fig. 2). And also the decrease of paramagnetism was observed at about 40 K by the susceptibility measurement, as shown in Fig. 3. The electrical-resistivity result shows metallic behavior again below about 90 K (Fig. 2). This indicates that the Fermi surfaces which were not destroyed by the CDW formation at about 110 K contribute to electrical conduction. The integrated intensity of the superlattice reflection at the reciprocal point $(\frac{2}{3}, -\frac{1}{3}, \frac{3}{7})$ showed no significant change around 40 K, as shown in Fig. 5. This suggests that the low-temperature phase transition is independent of the high-temperature one. The band calculation[4] indicates that there are three Fermi surfaces in Nb_3Te_4. These facts suggest that the anomaly at about 40 K comes from the phase transition due to the formation of a CDW which has a wave vector other than that of the high-temperature CDW. However we did not observe the corresponding superlattice reflections, although we made basic attempts to seek them. The amplitude of the CDW, if it exists, may be weak.

V. CONCLUSION

We have studied the phase transition around 110 K of Nb_3Te_4 by electrical resistivity, magnetic susceptibility, and x-ray diffraction measurements. This phase transition is first order, because hysteresis was observed in the electrical resistivity and in the integrated intensity of the superlattice reflection. It is due to the formation of the

CDW states with the commensurate wave vectors $\mathbf{q}_1=\frac{1}{3}\mathbf{a}^*+\frac{1}{3}\mathbf{b}^*+\frac{3}{7}\mathbf{c}^*$ and $\mathbf{q}_4=-\frac{1}{3}\mathbf{a}^*-\frac{1}{3}\mathbf{b}^*+\frac{3}{7}\mathbf{c}^*$, which form domains. The commensurate CDW was discussed in terms of Landau theory and we concluded that the space group of this state is C_3^1 $(P3)$ with $\sqrt{3}\,|\,\mathbf{a}\,|\times\sqrt{3}\,|\,\mathbf{a}\,|\times 7\,|\,\mathbf{c}\,|$ superlattice structure. In this structure the interchain interaction energy between the CDW's on the individual chains is minimized. The minimization of the interchain interaction energy leads to the ordering of the phases of the CDW's running on the individual zigzag Nb chains. As a result, the commensurate structure has a $\sqrt{3}\,|\,\mathbf{a}\,|\times\sqrt{3}\,|\,\mathbf{a}\,|$ basal-plane unit cell.

The anomaly at about 40 K in the electrical resistivity and the magnetic susceptibility may be ascribed to the formation of another CDW, which occurs through the nesting of remaining Fermi surfaces.

ACKNOWLEDGMENT

We are grateful to Dr. M. Izumi and T. Iwazumi for their assistance in the x-ray measurement and for helpful discussions.

APPENDIX: SYMMETRY TRANSFORMATION FOR THE ORDER PARAMETERS

The transformation properties of the order parameters Ψ_i with respect to the generators of the space group C_{6h}^2 are as follows:

$$\Psi_i\rightarrow\Psi_{i+1}\exp(iq_z\,|\,\mathbf{c}\,|/2)\ ,$$

$$\Psi_i^*\rightarrow\Psi_{i+1}^*\exp(-iq_z\,|\,\mathbf{c}\,|/2)\ ,$$

under $\{C_{6z}^+\,|\,0,0,\frac{1}{2}\}$, and

$$\Psi_i\rightarrow\Psi_{i+1}^*\exp(iq_z\,|\,\mathbf{c}\,|/2)\ ,$$

$$\Psi_i^*\rightarrow\Psi_{i+1}\exp(-iq_z\,|\,\mathbf{c}\,|/2)\ ,$$

under $\{\sigma_h\,|\,0,0,\frac{1}{2}\}$. Here $i+2=i$ and $q_z=3\,|\,\mathbf{c}^*\,|/7$. Moreover under the translation operation $\{E\,|\,1,0,0\}$,

$$\Psi_1\rightarrow\Psi_1\exp(i2\pi/3),\quad \Psi_2\rightarrow\Psi_2\exp(-i2\pi/3)\ ,$$

$$\Psi_1^*\rightarrow\Psi_1^*\exp(-i2\pi/3),\quad \Psi_2^*\rightarrow\Psi_2^*\exp(i2\pi/3)\ .$$

---

*Present address: Tsukuba Research Laboratory, Nippon Sheet Glass Co., Ltd., 5-4 Tokodai, Toyosato-machi, Tsukuba-gun, Ibaraki 300-26, Japan.

[1]E. Amberger, P. Polborn, P. Grimm, M. Dietrich, and B. Obst, Solid State Commun. **26**, 943 (1978).

[2]Y. Ishihara and I. Nakada, Solid State Commun. **45**, 129 (1983).

[3]K. Selte and A. Kjekshus, Acta Crystallogr. **17**, 1568 (1964).

[4]A. Oshiyama, Solid State Commun. **43**, 607 (1982); J. Phys. Soc. Jpn. **52**, 587 (1983).

[5]Y. Ishihara, I. Nakada, K. Suzuki, and M. Ichihara, Solid State Commun. **50**, 657 (1984).

[6]K. Suzuki, M. Ichihara, I. Nakada, and Y. Ishihara, Solid State Commun. **52**, 743 (1984).

[7]T. Sekine, Y. Kiuchi, M. Izumi, K. Uchinokura, R. Yoshizaki, and E. Matsuura, Proceedings of the International Conference on Science and Technology of Synthetic Metals, Kyoto, 1986 [Synth. Metals **19**, 875 (1987)].

[8]See, for example, C. Kittel, *Introduction to Solid State Physics*, 5th ed. (Wiley, New York, 1976), Chap. 14.

[9]D. Sahu and M. B. Walker, Phys. Rev. B **31**, 479 (1985).

[10]C. H. Chen, J. M. Gibson, and R. M. Fleming, Phys. Rev. Lett. **47**, 723 (1981).

[11]K. Suzuki, M. Ichihara, I. Nakada, and Y. Ishihara, Solid State Commun. **59**, 291 (1986).

[12]M. B. Walker, Can. J. Phys. **63**, 46 (1985).

[13]D. Sahu and M. B. Walker, Phys. Rev. B **32**, 1643 (1985).

[14]P. Bak and V. J. Emery, Phys. Rev. Lett. **36**, 978 (1976).